Atomistic Simulations of Nonequilibrium Crystal-Growth Kinetics from Alloy Melts

Yang Yang, Harith Humadi, Dorel Buta, Brian B. Laird, Deyan Sun, Jeffrey J. Hoyt, and Mark Asta

Phys. Rev. Lett. **107**, 025505 — Published 7 July 2011

DOI: 10.1103/PhysRevLett.107.025505

Atomistic Simulations of Non-Equilibrium Crystal-Growth Kinetics from Alloy Melts

Yang Yang,[1,2] Harith Humadi,[3] Dorel Buta,[4] Brian B. Laird,[1] Deyan Sun,[2] Jeffrey J. Hoyt,[3] and Mark Asta[5,4]

[1]*Department of Chemistry, Lawrence, KS, USA*
[2]*Department of Physics, East China Normal University, Shanghai, China*
[3]*Department of Materials Science and Engineering, McMaster University, Hamilton, ON, Canada*
[4]*Department of Chemical Engineering and Materials Science, University of California, Davis, CA, USA*
[5]*Department of Materials Science and Engineering, University of California, Berkeley, CA, USA*

Non-equilibrium kinetic properties of alloy crystal-melt interfaces are calculated by molecular-dynamics simulations. The relationships between interface velocity, thermodynamic driving force, and solute partition coefficient are computed and analyzed within the framework of kinetic theories accounting for solute trapping and solute drag. The results show a transition to complete solute trapping at high growth velocities, establish appreciable solute drag at low growth velocities, and provide insights into the nature of crystalline anisotropies and solute effects on interface mobilities.

There exists an extensive body of literature on the patterns and morphologies that can form when a near-equilibrium system evolves toward its equilibrium state [1]. By contrast, the understanding of systems far from equilibrium remains less advanced. A simple, yet illustrative, example of a far-from-equilibrium process is the rapid solidification of a highly undercooled melt. Rapid solidification occurs in many contexts such as laser-induced surface melting [2, 3], spray forming, and welding. The process can be exploited to form supersaturated solid solutions, metastable compounds, and glasses [4]. Due to advances in mesoscale simulation methods and a more detailed understanding of the thermodynamic properties of crystal-melt (CM) interfaces, substantial progress has been realized over the past decade in the modeling of solidification under near-equilibrium conditions [5]. By contrast, predictive models for rapid solidification remain less developed, due in part to the need for a more detailed understanding of the non-equilibrium properties of CM interfaces.

Under rapid-solidification conditions, the solute concentrations at the CM interface can deviate significantly from the values given by the equilibrium phase diagram, a phenomenon commonly referred to as *solute trapping* [2, 6–9]. Additionally, the growth of a crystal with a composition differing from that of its melt requires diffusion of solute across the CM interface; the free-energy dissipation associated with this trans-interface diffusion leads to a so-called *solute drag* effect that can significantly hinder the transformation rate (e.g., [10, 11]). While theoretical models [6, 7, 9, 10] have been extensively developed to account for such phenomena, several outstanding questions remain. Specifically, the theory for solute trapping developed by Galenko and Sobolev [7] (see also [12]) predicts a sharp transition to partitionless growth at a velocity dictated by the atomic-scale relaxation processes in the bulk liquid. By contrast, partitionless growth occurs only in the asymptotic limit of infinite growth velocities in the widely used theory of Kaplan and Aziz [6] and the most recent theory of Jackson *et al.* [9]. Further, solute drag is known to play an important role in a wide variety of solid-state transformations, and it remains unclear why it appears to be absent in the most detailed experimental studies of rapid solidification performed to date [2]. Finally, the magnitude and anisotropy of the CM interface mobility have been shown to be important factors in governing the morphology and growth velocities of dendrite solidification at high undercoolings [13], yet no information is currently available about the effect of solute atoms on these kinetic properties.

To address these issues, we present here a method for computing the kinetic properties of alloy CM interfaces by molecular dynamics (MD) simulations. The work extends earlier MD studies of solute trapping [14, 15], by providing a complete characterization of alloy CM interface kinetic properties, including the nature of crystalline anisotropies and the details of the velocity/driving-force relations. The approach is applied to two model systems with atomically-rough CM interfaces, which both crystallize in fcc crystal structures, but with differing degrees of equilibrium solute partitioning. The results show a transition to complete trapping at high growth velocities, establish the presence of appreciable solute drag at low velocities, and yield reduced interface mobilities in alloys relative to the corresponding pure elements.

To investigate the kinetic properties of alloy CM interfaces we consider two model systems. For the first the interatomic interactions take the form of the truncated Lennard-Jones (LJ) potentials considered by Huitema *et al.* [16], with the ϵ and σ values given in the supplementary information [17]. As shown in [17] the composition-temperature phase diagram for this system features negligible solubility of the solute species (B) in the solid (A), and thus displays a high degree of equilibrium solute partitioning. We consider also an embedded-atom-method model for Ni-Cu, with a phase diagram [18] that displays extensive solubility. Compared to the LJ system, Ni-Cu has a larger partition coefficient of $k_e \equiv x_s^e/x_l^e = 0.5$, where x_s^e and x_l^e denote equilibrium solidus and liquidus compositions, respectively. We discuss results of the LJ system in detail below, summarizing those for Ni-Cu for comparison purposes; further details of the Ni-Cu results

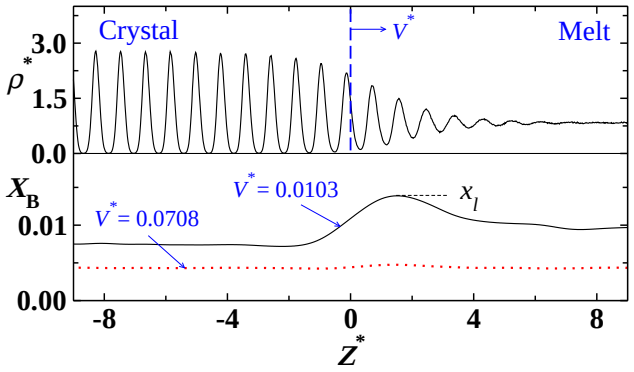

FIG. 1: (Color online). The averaged fine-grained profile for the total density across a CM interface with a velocity $V^* = 0.0103$ in the model LJ alloy system is given in the upper panel (the superscript * denotes LJ reduced units as defined in [17]). The smoothed, coarse-grained profile of the solute mole fraction is given in the lower panel, where the solid and dashed lines are for $V^* = 0.0103$ and $V^* = 0.0708$, respectively.

can be found in [17] and will be published elsewhere.

For both the LJ and Ni-Cu systems, crystallization simulations begin from equilibrated two-phase solid-liquid simulation cells, with each of the bulk phases prepared at their equilibrium phase-boundary compositions at a given temperature, and separated by CM interfaces oriented along {100} or {110}. For each equilibrated system, we induce crystal growth by decreasing the liquid solute composition and/or lowering the system temperature. Several replicas are prepared, which are given different initial velocity distributions, and allowed to evolve with independent trajectories. The positions of the CM interfaces during the growth simulations are monitored using a local structural order parameter. Equilibrium density, temperature, and composition profiles are derived by aligning each of the interfaces and computing averages in the reference frame of the moving interface. Details of the simulations and analysis are described in [17]. The top panel of Fig. 1 shows a representative fine-scale density profile, illustrating the diffuse nature of the CM interface. The bottom panel plots a smoothed coarse-grained solute concentration profile from a LJ simulation with a relatively low velocity (upper curve) and the highest velocity considered (lower curve). For the slower V results the peak in the concentration on the liquid side of the interface reflects partitioning of the solute. For the high V case the concentration profile is nearly flat, indicating clearly solute-trapping behavior.

Figure 2 plots MD results for the non-equilibrium partition coefficient $k(V) = x_s/x_l$. As described in detail in [17], we distinguish two cases in reporting these results, based on the following analysis. The interfacial region is divided into two parts, on the liquid and solid sides of the CM interface, and the solute composition in the former at a given time t_0 is compared with that in the latter at a later time $t_0 + \delta t$, where δt is the time required for the solid region to crystallize from the liquid. If the two compositions are statistically equivalent, we conclude that the solidification is partitionless, i.e., $k(V) = 1$. Otherwise, k is computed taking x_l as the peak composition on the liquid side of the interface, and x_s as the average concentration of the solid crystallized, as illustrated in Fig. 1. In Fig. 2, open-circle and filled-diamond symbols correspond to {110} and {100} interfaces, respectively, and show a statistically significant anisotropy.

We consider now a comparison of the $k(V)$ results with available theories for solute trapping: The continuous-growth model (CGM) of Kaplan and Aziz [6] is formulated by considering flux balances across a moving CM interface of width λ. The theory predicts that appreciable trapping will occur when the interface moves at a characteristic *trapping velocity*, V_D, equal to the speed at which a solute atom can traverse the interface: $V_D = D/\lambda$, where D is the liquid diffusivity. In the CGM the $k(V)$ function takes the following form (for dilute alloys):

$$k(V) = [k_e + (V/V_D^{CGM})]/[1 + (V/V_D^{CGM})] \qquad (1)$$

The local nonequilibrium model (LNM) of Galenko and Sobolev [7] is based on a similar approach as the CGM, but makes use of a generalized Fick's law that accounts for the finite relaxation time of the diffusion flux to its steady state. The LNM yields:

$$k(V) = \frac{k_e[1 - (V/V_B^{LNM})^2] + (V/V_D^{LNM})}{1 - (V/V_B^{LNM})^2 + (V/V_D^{LNM})} \qquad (2)$$

for V less than the bulk liquid diffusion speed V_B^{LNM} (related to the relaxation time for the diffusion flux), and $k(V) = 1$ for $V > V_B^{LNM}$. Finally, the most recent theory for solute trapping due to Jackson *et al.* [9] is derived using reaction rate theory to describe the the rate of atom attachments to the active sites of a sharp CM interface. For rough interfaces the theory yields:

$$k(V) = k_e^{1/(1+AV)}. \qquad (3)$$

where $1/A$ represents the characteristic velocities above which $k(V)$ deviates strongly from k_e.

In the lower panel of Fig. 2 the solid and dashed lines are least-squares fits of the CGM and Jackson models to all of the the LJ MD data. Both theories fit the data for the lower velocities, where $k \neq 1$ with comparable accuracy. However, the MD data at the highest V, which is determined to be partitionless by the analysis of the MD data, is naturally underestimated by these theories which predict $k \to 1$ as asymptotic behavior for $V \to \infty$. In the upper panel of Fig. 2 the solid lines represent a fit of the LNM model to the data for which $k \neq 1$. The fits of the {100} and {110} data predict a transition to partitionless solidification at a velocity V_B^{LNM} that is independent of interface orientation, consistent with

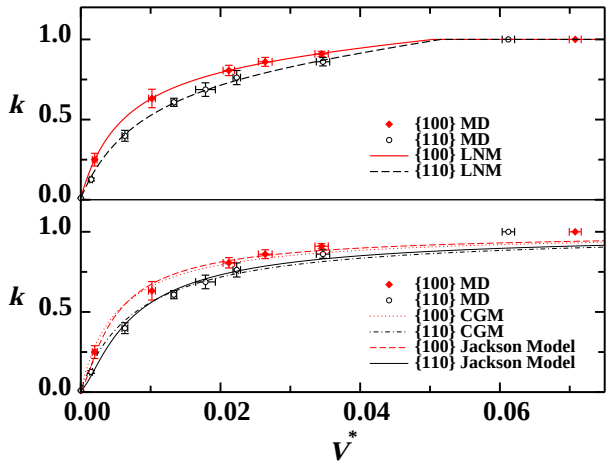

FIG. 2: (Color online). MD calculated values of the partition coefficient (k) are plotted versus interface velocity (V^*, in reduced units) with open and filled symbols for {110} and {100} interface orientations, respectively. Lines are fits of the MD data to available theories (see text).

the LNM theory in which this parameter is controlled by relaxation processes in the bulk liquid.

Table I lists the solute-trapping model parameters for the theoretical models, derived from a fit to both the LJ and Ni-Cu MD results. An appreciable anisotropy is found for the trapping velocities for the LJ systems, with {110}interfaces trapping at higher velocities than {100}. For Ni-Cu, the statistical uncertainties are significantly higher due to the larger value of k_e in this system. However, the differences in trapping velocities for {100} and {110} interfaces are smaller for Ni-Cu than the LJ system, indicating that the anisotropy in this property appears to be system dependent.

The second function required to define the growth kinetics in a sharp-interface theory is the relationship between V and the driving force for interface migration, ΔG_m. For the rough CM interfaces considered here this relationship is taken as linear:

$$V = M\Delta G_m \tag{4}$$

where M is the interface mobility. The driving force is commonly written as $\Delta G_m = \Delta G_{chem} - \Delta G_D$, where ΔG_{chem} is the total chemical free energy change due to solidification, and ΔG_D is the free energy dissipated due to solute drag (ΔG_D). Following Hillert [10] we have:

$$\Delta G_m = x_{\rm eff}\Delta\mu_B + (1 - x_{\rm eff})\Delta\mu_A \tag{5}$$

where $\Delta\mu_B$ denotes the difference between the chemical potential of the solute species B in the solid versus the liquid phase, and similarly for $\Delta\mu_A$. The effective composition $x_{\rm eff}$ is defined as:

$$x_{\rm eff} = (1 - f)x_s + fx_l \tag{6}$$

where the limit $f = 0$ corresponds to $\Delta G_D = 0$, and increasing values of f correspond to increasing values of ΔG_D. In the version of the CGM that accounts for solute drag $f = 1$, while in the model of Jönsson and Ågren [19] it was assumed $f = 1/2$. The values of f can be derived from diffuse-interface theories [10], where its exact value depends on the assumptions concerning the nature of the variations of the solute concentration and diffusion coefficient across the CM interface. For the phase-field model developed by Ahmad *et al.* [8], $f = 24/35$.

The top panel of Fig. 3 plots the LJ-MD values of V versus ΔG_m, neglecting solute drag, i.e., assuming $f = 0$, such that $\Delta G_m = \Delta G_{chem}$. A linear least squares fit of the data (following Eq. (4)) is seen to overestimate V for the slowest growth rates and underestimate the data at the highest velocities. These discrepancies can be attributed to the effects of solute drag. Specifically, by its definition, ΔG_D is significant only at the slower growth rates where there is appreciable solute partitioning at the CM interface. For the slowest velocities, solute drag has the effect of reducing ΔG_m, while leaving the driving force for the highest velocity points (where solidification is essentially partitionless) unchanged. The lower panel of Fig. 3 shows the best fit of the LJ MD data accounting for solute drag using Eqs. (4)-(6). A much improved fit of the data over the entire velocity range is now obtained using a constant, velocity independent value of f. The fitted value of f are given in Table I for both the LJ and Ni-Cu systems. The values of $f \approx 0.3$ are smaller than but comparable in magnitude to those derived from the diffuse interface theories mentioned above.

The slopes of the best-fit lines in the bottom panel of Fig. 3 are the interface mobilities (M) defined in Eq. (4). The values of M obtained from fits to the LJ and Ni-Cu systems, accounting for solute drag, are listed in Table I. As found previously for elemental systems with fcc crystal structures (e.g., [5] and references therein), the {100} orientation features an appreciably larger value of M relative to {110} for the LJ system (the statistical uncertainties for the Ni-Cu system are seen in Table I to be too large to deduce anisotropy values). The kinetic anisotropy $M_{100}/M_{110} = 1.48(2)$ derived for the LJ system is in the range of values obtained in previous MD simulations for fcc-based pure element systems [5]. The magnitudes of M obtained for the LJ alloy system can be compared directly to those for the pure solvent species (element A), obtained with the same potentials. The kinetic anisotropy for the alloy is statistically equivalent to the value of $M_{100}/M_{110} = 1.58(9)$ obtained for the pure solvent. However, the magnitudes of the alloy mobilites for each orientation are reduced by approximately 25 % relative to the pure solvent.

Despite the fact that solute trapping and solute drag are known to play crucial roles in the microscopic mechanisms underlying phase transformations in alloys, very few experiments have examined both phenomena in the

TABLE I: Values of the interface kinetic parameters, defined in Eqs. (1)-(6), from least-squares fits to the MD data for {100} and {110} interface orientations. Numbers in parentheses are 95 % confidence intervals on the last significant figures.

	Lennard-Jones						Ni-Cu					
	V_D^{CGM}	V_D^{LNM}	V_B^{LNM}	A	M	f	V_D^{CGM}	V_D^{LNM}	V_B^{LNM}	A	M	f
	$(\sqrt{\epsilon/m}\times 10^{-3})$			$\sqrt{m/\epsilon}$	$\sqrt{1/m\epsilon}$		(m/s)			s/m	m/s-eV	
{100}	5.3(2)	6.3(3)	50(3)	10.5(4)$\times 10^2$	1.67(1)	0.36(1)	1.3(3)	1.4(4)	15(4)	1.1(3)	58(16)$\times 10^2$	0.3(2)
{110}	8.0(1)	9.6(2)	51(2)	6.9(1) $\times 10^2$	1.13(1)	0.32(2)	1.5(3)	1.6(4)	21(10)	1.0(2)	49(9) $\times 10^2$	0.3(2)

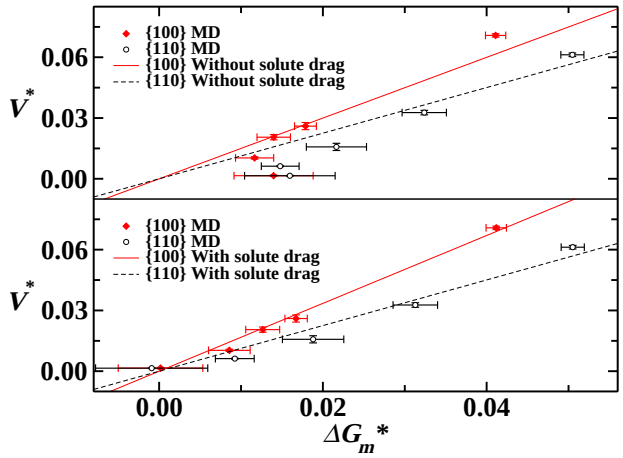

FIG. 3: (Color online). The upper and lower panels plot MD calculated velocities versus driving force with and without solute drag, respectively. Lines are fits to Eq. (4).

context of crystal growth from the melt, and none have probed the large range of velocities required to investigate the dynamic transition to complete trapping. Here we have calculated the kinetic properties of atomically-rough CM interfaces directly by MD simulations. Results for solute trapping at high V are consistent with the theory of Ref. [7], which predicts an abrupt transition to partitionless solidification at a velocity that is independent of interface orientation. Further, we demonstrate anisotropy in the CM interface mobility comparable to that obtained for elemental fcc-forming systems, while showing a tendency for reduced values of M in alloys relative to corresponding pure element systems. The MD data indicates the presence of appreciable solute drag for the systems considered. This finding is interesting given that no measurable solute drag was found in the analysis of detailed experimental measurements of the Si(As) system presented in Ref. [2]. Further investigations of solute drag are thus warranted, as the current results and those in Ref. [2] suggest that the effect may be significantly different for systems with (directional) covalent versus metallic bonding.

DB and MA were supported by the US Department of Energy, Office of Basic Energy Sciences, under contract DE-FG02-06ER46282. YY and DS were supported by the National Natural Science Foundation of China. HH and JH were supported by a Natural Sciences and Engineering Research Council of Canada Discovery Grant, and SHARCNET, Ontario, Canada. BBL was supported by the National Science Foundation, grant CHE-0957102. We further acknowledge support from the DOE Computational Materials Science Network program, and the National Research Scientific Computing Center (DOE Office of Science contract DE-AC02-05CH11231).

[1] J. P. Gollub and J. S. Langer, Rev. Mod. Phys. **71**, S396 (1999).
[2] J. A. Kittl *et al.*, Acta Mater. **48**, 4797 (2000).
[3] W.-L. Chan *et al.*, Phys. Rev. Lett. **102**, 095701 (2009).
[4] D. Herlach, P. Galenko and D. Holland-Moritz, *Metastable Solids from Undercooled Melts* (Elsevier, 2007).
[5] M. Asta *et al.*, Acta Mater. **57**, 941 (2009).
[6] M. J. Aziz and T. Kaplan, Acta Metall. **36**, 2335 (1988).
[7] P. Galenko and S. Sobolev, Phys. Rev. E **55**, 343 (1997).
[8] N. A. Ahmad *et al.*, Phys. Rev. E **58**, 3436 (1998).
[9] K. A. Jackson, K. M. Beatty and K. A. Gudgel, J. Cryst. Growth **271**, 481 (2004).
[10] M. Hillert, Acta Mater. **47**, 4481 (1999).
[11] M. Buchmann and M. Rettenmayr, Scripta Mater. **57**, 169 (2007).
[12] P. K. Galenko and D. M. Herlach, Phys. Rev. Lett. **96**, 150602 (2006).
[13] J. Bragard *et al.*, Interface Sci. **10**, 121 (2002).
[14] Q. Yu and P. Clancy, J. Cryst. Growth **149**, 45 (1995).
[15] F. Celestini and J.-M. Debierre, Phys. Rev. B **62**, 14006 (2000).
[16] H. E. A. Huitema, B. van Hengstum and J. P. van der Eerden, J. Chem. Phys. **111**, 10248 (1999).
[17] See EPAPS Document No. for additional information. For more information on EPAPS, see http://www.aip.org/pubservs/epaps.html
[18] E. B. Webb and J. J. Hoyt, Acta Mater. **56**, 1802 (2008).
[19] B. Jönsson and J. Ågren, J. Less-Common Metals **145**, 153 (1988).